Generalized KVL-KCL Formulation for Coupled Electromagnetic-Circuit Simulation with Surface Integral Equations

Yong Wang, Dipanjan Gope, Vikram Jandhyala and C.J. Richard Shi
jandhyala@ee.washington.edu

Dept of EE, University of Washington
Seattle WA, 98195-2500

UWEE Technical Report
Number UWEETR-2003-0017
July 16, 2003

Department of Electrical Engineering
University of Washington
Box 352500
Seattle, Washington 98195-2500
PHN: (206) 543-2150
FAX: (206) 543-3842
URL: http://www.ee.washington.edu

Generalized KVL-KCL Formulation for Coupled Electromagnetic-Circuit Simulation with Surface Integral Equations

Yong Wang, Dipanjan Gope, Vikram Jandhyala and C.J. Richard Shi

Dept of Electrical Engineering, University of Washington, Seattle WA 98195
Email: jandhyala@ee.washington.edu, Ph: 206-543-2186, Fax: 206-543-3842

University of Washington, Dept. of EE UWEETR-2003-0017
July 16, 2003

In this paper, a new formulation for coupled electromagnetic-circuit simulation is presented. The formulation employs full-wave integral equations to model the electromagnetic (EM) behavior of 2D or 3D structures while using modified nodal analysis (MNA) to model circuit interactions. A coupling scheme based on charge and current continuity and potential matching, realized as a generalization of Kirchoff's voltage and current laws, ensures that the EM and circuit interactions can be formulated as a seamless system. While rigorous port models for EM structures can be obtained using the approach discussed herein, it is shown that the coupling paradigm can reveal additional details of the EM-circuit interactions and can provide a path to analysis-based design iteration.

I. Introduction

With the rapidly increasing interest in applications such as radio frequency wireless communication and high-speed data processing, electronic systems are required to work at progressively higher frequencies [1]. As the operating frequencies enter the GHz range, phenomena such as cross talk, power-ground-plane voltage bounce, and substrate losses can no longer be neglected. In order to design high-performance systems with fast times-to-market, it is essential to be able to analyze whole or part of the system at one fundamentally deeper level of physics: distributed electromagnetic (EM) field analysis needs to be rigorously and seamlessly included as an addition to traditional circuit simulation.

In existing literature, several methods have been developed to model and simulate coupled circuit and EM problems. Those based on finite difference time domain (FDTD) [2-4] are effective for time-domain analysis. However, FDTD is inherently not suitable for frequency-domain analysis. Furthermore, FDTD requires the discretization of the 3D space where the object under study resides, which can lead to substantially more system unknowns than in surface-based methods [5]. The Finite Element Method (FEM) has been applied to both time domain and frequency domain coupled EM-circuit simulation using schemes including port models [6], via paralleling each coupling circuit element to an FEM edge [7], or through a fully-coupled approach [8]. Transmission line methods and other analytical approaches [9] are usually much faster than the numerical based methods and can be easily coupled to circuit simulation. However, they are not general enough for analyzing irregular structures. In recent years, methods based on integral equations have gained momentum. Among them, the partial element equivalent circuit

(PEEC) approach [10] has been widely used to study coupled circuit-EM problems. Very recently, non-orthogonal and generalized PEEC methods have been developed [11,12]. By representing all the interactions using equivalent SPICE-compatible RLC elements and controlled sources, PEEC can solve the coupled circuit-EM problem using a traditional SPICE-like circuit simulator. However, due to the dense nature of the interactions and the fact that SPICE is tuned for solving sparse matrices, direct PEEC is limited to problems with a relatively small number of unknowns [13], although, recently, fast methods in conjunction with PEEC are being developed [14]. The PEEC method itself was inspired by EM integral equations. Such equations, solved by the method of moments (MoM) [5], can be used for distributed effects simulation of arbitrarily-shaped structures with surface-only formulations. However when non-trivial lumped circuits are simultaneously present, previous work can only solve the coupled problem based on port models through several steps. First port parameters are calculated using an EM simulator, then curve fitting or model order reduction techniques are used to generate an equivalent circuit model, followed by circuit simulation to estimate complete electrical performance of the system. The port-model based approach has several limitations: First, for complex multi-port structures with frequency dependent material properties, deriving the equivalent passive network within a given accuracy is still an area of current research [15]. Second, after the EM structure is converted to port model, information about the details of the electromagnetic field distribution in the structure will be lost, such information could otherwise provide useful insights into the problem under study and be useful in design iterations.

This paper presents a new and complementary approach to the formulation and solution of the coupled EM-circuit problem. EM conducting structures and lumped-element circuits are formulated jointly using one system matrix, in a form amenable to existing fast iterative numerical solvers such as those based on fast multipole methods, FFT methods, and low-rank decompositions, as well as emerging fast direct solvers [16]. Solving the EM and circuit simultaneously not only permits more detailed field information, but also obviates the necessity of generating port models and thus automates the design flow. The proposed method is inherently hierarchical, and provides seamless transitions between circuit and EM depending on the level of details required.

The EM formulation used in this paper is a full-wave MoM approach using surface triangular tesselations. Since Rao-Wilton-Glisson (RWG) basis functions [5] associated with triangular meshes do not make assumptions about current flow directions as the classical volumetric PEEC does, the adopted approach is suitable to model arbitrarily shaped structures often found in microwave and radio frequency applications. Furthermore, frequency dependent effects such as skin effect can be modeled easily via employing lossy media's Green's functions in a two-region formulation without frequency dependent meshing [17].

For the circuit sub-system, the standard modified nodal analysis matrix is formulated. Kirchoff's Current Law (KCL) is enforced for each circuit node and Kirchoff's Voltage Law (KVL) is applied to branches containing voltage sources. Areas of EM structures where the circuit connections are made are defined as *contact* regions. Associated with each *contact* is one coupling current that is introduced as an additional system unknown. The coupling scheme is based on charge and current continuity equations and potential

matching with the assumption that circuit voltage is equal to the EM scalar potential at a contact region.

The rest of the paper is organized as following: Section II introduces the formulation of surface-based electric field integral equations (EFIE) for EM structures, and modified nodal analysis (MNA) equations for lumped-element circuits. Implementation of the coupled method using RWG basis functions is presented in Section III. Section IV discusses port model derivation and parameter extraction. Numerical examples for a low noise amplifier, power/ground plane bounce modeling, and a coupled package are given in section V. Section VI discusses conclusions.

II. Coupled EM-Circuit Formulation

This section presents a generalized KCL-KVL formulation for simulation of coupled EM-circuit problems. A typical high-speed microelectronic system layout consists of both lumped circuits and sections requiring distributed EM simulation. For modeling purposes, the circuit section is abstracted by a topology-based domain wherein signals propagate along idealized conduction paths between lumped-circuit elements, while the EM section is represented by a geometry-based domain wherein signals propagate in 3D space and materials. The two domains couple to each other through contact interfaces where a circuit node is associated with an EM contact surface. As will be shown in this paper, this interface can be rigorously defined using a generalized version of Kirchoff's voltage and current laws (KVL and KCL).

Consider Figure 1 that shows a lumped circuit connected through a contact surface to a 3D geometric object. For 3D conducting objects connected to arbitrary circuit elements

and sources and, optionally, illuminated by incident fields, the boundary condition for the electric field on the surface *S* of the object is

$$\left(\mathbf{E}^s(\mathbf{J}) + \mathbf{E}^i\right)_{\tan} = Z_s \mathbf{J} \tag{2.1}$$

where $\mathbf{E}^s$ is the scattered electric field produced by the induced equivalent surface current $\mathbf{J}$, $\mathbf{E}^i$ is the incident electric field, subscript tan denotes the tangential components on *S*, and Z_s represents the surface impedance

$$Z_s = \sqrt{\frac{jwm}{2s}} \tag{2.2}$$

where w is angular frequency, m and σ are the permittivity and conductivity of the material respectively. Note that surface impedance is a valid approximation to the behavior of fields internal to conductors only for frequencies where the skin depth is smaller than the dimension of the cross section of conductors. At lower frequencies, if a surface integral formulation is used, more accurate modeling of the lossy media Green's function within the conductor is required, as discussed in [18]. In terms of potentials, the electric field can be written as:

$$\mathbf{E}^s(\mathbf{J}) = -jw\mathbf{A} - \nabla\Phi \tag{2.3}$$

where the vector potential $\mathbf{A}$ is defined as:

$$\mathbf{A}(\mathbf{r}) = \frac{m}{4p}\int_S \frac{e^{-jk|\mathbf{r}-\mathbf{r}'|}\mathbf{J}(\mathbf{r}')}{|\mathbf{r}-\mathbf{r}'|}ds' \tag{2.4a}$$

the scalar potential Φ is defined as:

$$\Phi(\mathbf{r}) = \frac{1}{4pe}\int_S \frac{e^{-jk|\mathbf{r}-\mathbf{r}'|}r(\mathbf{r}')}{|\mathbf{r}-\mathbf{r}'|}ds' \tag{2.4b}$$

where $\mathbf{r}$ and $\mathbf{r}'$ are observation and source locations, respectively. $\mathbf{J}$ and r represent the equivalent surface current density and surface charge density, respectively; m, e, k are the permeability, permittivity, and wave number, respectively, of the homogeneous medium enclosing the object.

The concept of a *contact* is introduced here. Referring to Figure 2, the surface S is divided into two sub-surfaces, denoted by S_{CK} and S_{EM} such that:

$$S_{EM} \cup S_{CK} = S \tag{2.5a}$$

and

$$S_{EM} \cap S_{CK} = f \tag{2.5b}$$

On S_{EM} the standard continuity equation relating the surface current $\mathbf{J}$ and surface charge r holds:

$$\nabla_s \cdot \mathbf{J}(\mathbf{r}) + jwr(\mathbf{r}) = 0 \ , \forall \mathbf{r} \in S_{EM} \tag{2.6a}$$

or

$$r(\mathbf{r}) = -\frac{\nabla_s \cdot \mathbf{J}(\mathbf{r})}{jw} \ , \ \forall \mathbf{r} \in S_{EM} \tag{2.6b}$$

where ∇_s represents the surface divergence.

On S_{CK}, the continuity equation is altered due to the existence of injected circuit currents. This current introduces an additional source term in the continuity equation and thus affects the distribution of both surface currents and surface charges. Let S_{CK} be comprised of M disjoint surfaces $S_{CK}^m \quad m = 1,...,M$, each such unique sub-surface S_{CK}^m is termed one of M *contacts*. On S_{CK}^m, the modified continuity equation has the following form:

$$\nabla_s \cdot \mathbf{J}(\mathbf{r}) + jw r(\mathbf{r}) = J_c^m(\mathbf{r}),\ \forall \mathbf{r} \in S_{CK}^m \tag{2.7a}$$

or

$$r(\mathbf{r}) = -\frac{\nabla_s \cdot \mathbf{J}(\mathbf{r})}{jw} + \frac{J_c^m(\mathbf{r})}{jw},\ \forall \mathbf{r} \in S_{CK}^m,\ m = 1,....,M \tag{2.7b}$$

where J_c^m represents the scalar volumetric current density produced on S_{CK}^m via a circuit interconnection.

Substitute Eqn. (2.5, 2.6, 2.7) into Eqn. (2.3, 2.4), we have:

$$\begin{aligned}\mathbf{E}^s(\mathbf{J}) = &- jw\frac{m}{4p}\int_S \frac{e^{-jk|\mathbf{r}-\mathbf{r}'|}\mathbf{J}(\mathbf{r}')}{|\mathbf{r}-\mathbf{r}'|}ds' - \nabla\frac{1}{4pe}\int_S \frac{e^{-jk|\mathbf{r}-\mathbf{r}'|}r(\mathbf{r}')}{|\mathbf{r}-\mathbf{r}'|}ds' \\ &- \nabla\frac{1}{4pe}\sum_{m=1}^{M}\int_{S_{CK}^m}\frac{e^{-jk|\mathbf{r}-\mathbf{r}'|}J_c^m(\mathbf{r}')}{jw|\mathbf{r}-\mathbf{r}'|}ds'\end{aligned} \tag{2.8}$$

The last two terms represent the contribution to the field produced by the gradient of the scalar potential, which in turn is produced by the equivalent surface charge density. The charge density itself is produced by $\nabla_s \cdot \mathbf{J}/jw$ over S_{EM}, and by $\left(\nabla_s \cdot \mathbf{J} - J_c^m\right)/jw$ over S_{CK}^m. Therefore the current density introduced by the circuit interconnection produces an additional source or sink of charge that alters the scalar potential and the resulting electric field.

The current density J_c^m is a system unknown that is determined by the solution of the coupled circuit-EM system. An additional system equation can also be constructed, based on a generalized KVL that equates the scalar potential produced on electrically small contacts S_{CK}^m to the voltage of the circuit node associated with the interconnection at S_{CK}^m:

$$V_n = \frac{1}{4pe}\left(\int_S \frac{e^{-jk|\mathbf{r}-\mathbf{r}'|}r(\mathbf{r}')}{|\mathbf{r}-\mathbf{r}'|}ds' + \sum_{m=1}^{M}\int_{S_{CK}^m}\frac{e^{-jk|\mathbf{r}-\mathbf{r}'|}J_c^m(\mathbf{r}')}{jw|\mathbf{r}-\mathbf{r}'|}ds'\right),\ \forall \mathbf{r} \in S_{CK}^n,\ n=1,...,M \tag{2.9}$$

where V_n corresponds to node voltages associated with circuit nodes connected to *contacts.*

The *contact* as defined above is inherently an electrically small surface, i.e. its dimensions are small compared to the wavelength of signals in a microelectronic system. Larger *contacts* can be defined by associating several circuit nodes with neighboring contact regions, thereby not enforcing erroneous constant potential over electrically large regions.

The final self-consistency condition, in addition to scalar potential matching, is a generalized KCL that ensures that the coupling current will contribute one additional term I_c^n to the KCL based circuit equation associated with circuit node n

$$\sum_{i=1}^{B} I_i + I_c^n = 0 \tag{2.10}$$

where I_i is the current of the i^{th} branch, B is the total number of circuit branches connected to circuit node n. Figure 3 shows the connection scheme for the EM-circuit interface.

We notice that while other approaches such as delta gap methods or wire basis functions can be used to describe the coupling between the circuit and EM, they are not general enough for modeling the connection with arbitrary lumped circuits, or need artificial parameters such as basis function lengths, directions and radii that are not consistent with topology-only circuit sections.

III. Integral Equation with RWG basis functions

The self-consistent coupled EM-circuit equations described in Section II are valid for arbitrary basis functions for modeling surface currents using surface integral

formulations. In this section, the method is expressed in more detail for the popular edge-based Rao-Wilton-Glisson (RWG) spatial basis functions [5] that rely on a triangular tessellation of the surface S. An RWG function $\mathbf{f}_n(\mathbf{r})$, defined over two triangles with a common edge n, used to approximate the spatial distribution of current density has the well-known form

$$\mathbf{f}_n(\mathbf{r}) = \begin{cases} \dfrac{l_n}{2A_{n+}} \boldsymbol{\rho}_{n+} & \mathbf{r} \in T_{n+} \\ \dfrac{l_n}{2A_{n-}} \boldsymbol{\rho}_{n-} & \mathbf{r} \in T_{n-} \end{cases} \tag{3.1}$$

where l_n is the length of the n^{th} edge, $A_{n+/-}$ is the area of triangle $T_{n+/-}$ and $\boldsymbol{\rho}_{n+/-}$ is the vector pointing to or from location $\mathbf{r}$ in triangle $T_{n+/-}$. Figure 4 illustrates the definition of RWG basis functions. As a consequence of the above form, the charge density in each pair of triangles is modeled as piece-wise constant:

$$\nabla \cdot \mathbf{f}_n(\mathbf{r}) = \begin{cases} \dfrac{l_n}{A_{n+}} & \mathbf{r} \in T_{n+} \\ -\dfrac{l_n}{A_{n-}} & \mathbf{r} \in T_{n-} \end{cases} \tag{3.2}$$

The surface current density is expanded using RWG functions as

$$\mathbf{J}(\mathbf{r}) \cong \sum_{i=1}^{N_e} I_i \mathbf{f}_i(\mathbf{r}) \tag{3.3a}$$

where I_i represents the coefficient of the i^{th} RWG basis function, and N_e is the total number of non-boundary edges. For consistency with RWG basis functions, the charge associated with the coupling current density is modeled using piece-wise constant functions h (that have a value of unity on a given triangle and zero elsewhere) over each contact triangle

$$J_{c,n}^{m}(\mathbf{r}) \cong \sum_{m=1}^{M} \sum_{n=1}^{N_{pCK}^{m}} J_n^m \, h_n^m(\mathbf{r}) \tag{3.3b}$$

Equation (2.9) is then expressed as

$$\begin{aligned}\mathbf{E}^s(\mathbf{r}) = &- jw \frac{m}{4p} \sum_{i=1}^{N_e} I_i \int_{T_{i+} \cup T_{i-}} \frac{e^{-jk|\mathbf{r}-\mathbf{r}'|}\mathbf{f}_i(\mathbf{r}')}{|\mathbf{r}-\mathbf{r}'|} ds' + \nabla \frac{1}{4pe} \sum_{i=1}^{N_e} I_i \int_{T_{i+} \cup T_{i-}} \frac{e^{-jk|\mathbf{r}-\mathbf{r}'|}\nabla_s \cdot \mathbf{f}_i(\mathbf{r}')}{jw|\mathbf{r}-\mathbf{r}'|} ds' \\ &- \nabla \frac{1}{4pe} \sum_{m=1}^{M} \sum_{n=1}^{N_{pCK}^{m}} J_n^m \int_{T_{nCK}^{m}} \frac{e^{-jk|\mathbf{r}-\mathbf{r}'|} h_n^m(\mathbf{r}')}{jw|\mathbf{r}-\mathbf{r}'|} ds'\end{aligned} \tag{3.4}$$

where N_e is the total number of non-boundary edges, N_{pCK}^{m} is total number of triangles on contact m, T_{nCK}^{m} denotes the n^{th} triangle on contact m that is used for circuit connection. Also, T_{i+} and T_{i-} are the positive and negative triangle associated with the i^{th} RWG function. To solve for the unknown coefficients, the expression in Eqn. (3.4) is substituted into Eqn. (2.1), and tested with the RWG functions to yield

$$jw \langle \mathbf{f}_n, \mathbf{A}(\mathbf{r}) \rangle_{\tan} + \langle \mathbf{f}_n, \nabla\Phi(\mathbf{r}) \rangle_{\tan} = -\langle \mathbf{f}_n, Z_s \mathbf{J} \rangle_{\tan} + \langle \mathbf{f}_n, \mathbf{E}^i \rangle_{\tan}, \; n = 1,.., N_e \tag{3.5}$$

where $\langle .,. \rangle$ denotes a spatial dot-product, and testing of the vector potential yields

$$\langle \mathbf{f}_n, \mathbf{A}(\mathbf{r}) \rangle = \frac{m}{4p} \sum_{i=1}^{N_e} I_i \left\langle \mathbf{f}_n, \int_{T_{i+} \cup T_{i-}} \frac{e^{-jk|\mathbf{r}-\mathbf{r}'|}\mathbf{f}_i(\mathbf{r}')}{|\mathbf{r}-\mathbf{r}'|} ds' \right\rangle \tag{3.6}$$

The testing of the scalar potential is the result of the sum of two potential contributions, from the EM surface current, Φ_s

$$\langle \mathbf{f}_n, \nabla\Phi_s(r) \rangle = -\frac{1}{4pe} \sum_{i=1}^{N_e} I_i \left\langle \nabla \cdot \mathbf{f}_n, \int_{T_{i+} \cup T_{i-}} \frac{e^{-jk|\mathbf{r}-\mathbf{r}'|}\nabla_s \cdot \mathbf{f}_i(\mathbf{r}')}{jw|\mathbf{r}-\mathbf{r}'|} \right\rangle \tag{3.7}$$

and from the coupling current, Φ_c

$$\left\langle \mathbf{f}_n, \nabla\Phi_c(r) \right\rangle = \frac{1}{4pe} \sum_{m=1}^{M} \sum_{i=1}^{N_{pCK}^m} J_i^m \left\langle \nabla\cdot\mathbf{f}_n, \int\limits_{T_{iCK}^m} \frac{e^{-jk|\mathbf{r}-\mathbf{r}'|} h_i^m(\mathbf{r}')}{jw|\mathbf{r}-\mathbf{r}'|} \right\rangle \tag{3.8}$$

The surface impedance contribution is local, and has non-zero values only for those combinations of basis and testing functions that share at least one triangle. Therefore the contribution is a sparse matrix where each column has at most five non-zero entries.

$$\left\langle \mathbf{f}_n, Z_s\mathbf{J} \right\rangle = Z_s \sum_{i=1}^{N_e} I_i \left\langle \mathbf{f}_n, \mathbf{f}_i \right\rangle \quad n,i \text{ share a common Trangle} \tag{3.9}$$

Finally, any incident electric field is tested as in the term $\left\langle \mathbf{f}_n, \mathbf{E}^i \right\rangle$.

The next set of equations is obtained by enforcing

$$V_n = -\frac{1}{4pe\,jw} \left(\sum_{i=1}^{N_e} I_i \left\langle h_n^m, \int\limits_{T_{i+}\cup T_{i-}} \frac{e^{-jk|\mathbf{r}-\mathbf{r}'|} \nabla_s\cdot\mathbf{f}_i(\mathbf{r}')}{|\mathbf{r}-\mathbf{r}'|} ds' \right\rangle + \sum_{m=1}^{M} \sum_{k=1}^{N_{pCK}^m} J_n^m \int\limits_{S_{CK}^m} \frac{e^{-jk|\mathbf{r}-\mathbf{r}'|} h_n^m(\mathbf{r}')}{jw|\mathbf{r}-\mathbf{r}'|} ds' \right), \ \forall \mathbf{r} \in S_{CK}^n, \ n=1,\ldots,M \tag{3.10}$$

and by enforcing Eqn. (3.3b). Substituting Eqn. (3.7-3.10) in Eqn. (3.6) leads to the matrix format of the coupled EM-circuit system:

$$\begin{bmatrix} \mathbf{Z_{11}} & \mathbf{Z_{12}} & \mathbf{0} \\ \mathbf{Z_{21}} & \mathbf{Z_{22}} & \mathbf{C} \\ \mathbf{0} & \mathbf{C^T} & \mathbf{MNA} \end{bmatrix} \begin{bmatrix} \mathbf{i} \\ \mathbf{j_c} \\ \mathbf{ckt} \end{bmatrix} = \begin{bmatrix} \mathbf{v_{em}} \\ \mathbf{0} \\ \mathbf{v_{ckt}} \end{bmatrix} \tag{3.11}$$

where $\mathbf{Z_{11}}$ is the regular method of moments matrix whose elements can be interpreted as equivalent partial impedances if a comparison with surface-based PEEC is desired. The partial inductances, capacitances, and resistances are equivalent to the terms in Eqn. (3.7-3.9). The remaining three dense EM matrices define the *contact*. Matrix $\mathbf{Z_{12}}$ represents the electric field contribution due to the contact coupling current, and matrix $\mathbf{Z_{21}}$ denotes the potential contribution from the EM surface current at the *contacts*. Finally, matrix $\mathbf{Z_{22}}$ represents the contribution to contact potentials due to contact coupling currents.

This two-by-two system is a self-consistent definition of the EM interactions, and of the *contact* defining where the EM object connects with a circuit section. To complete the coupled formulation, a sparse, rectangular matrix $\mathbf{C}$ is introduced as connection matrix to enforce generalized KCL and KVL. This matrix has one non-zero element per row to select the potential of the circuit node associated with a contact triangle. The transpose matrix $\mathbf{C}^T$ selects the coupling current and adds it to the KCL equation of the circuit node at the *contact*. The **MNA** matrix represents circuit interactions for linear R-L-C elements and nonlinear elements such as diodes and transistors. The system unknowns $\mathbf{i}$, $\mathbf{j}_c$ and **ckt** relate to surface equivalent currents, coupling currents and circuit voltages/currents respectively. The right-hand-side excitation vector consists of the tested incident EM field $\mathbf{v}_{em}$, and the strengths of independent voltage and current sources $\mathbf{v}_{ckt}$ [19].

IV. Port Model and Parameter Extraction

Equations (3.3b, 3.10) permit sufficient flexibility in solution in order to aid in iterative design processes. In effect, iterations on one of the sections are facilitated by exploiting the constancy on the other section through a Schur complement. The equivalent of terminal models for each domain can be extracted and referred multiple times as shown next.

When structures to be analyzed with EM analysis remain unchanged and circuit parameters and topologies vary during design iterations, an *EM contact* model is generated. By combining the first two equations and unknowns, equation (3.11) can be rewritten as:

$$\begin{pmatrix} \mathbf{EM} & \mathbf{C'} \\ \mathbf{C'}^{\mathrm{T}} & \mathbf{MNA} \end{pmatrix} \begin{pmatrix} \mathbf{i'} \\ \mathbf{ckt} \end{pmatrix} = \begin{pmatrix} \mathbf{v}_{\mathbf{em'}} \\ \mathbf{v}_{\mathbf{ckt}} \end{pmatrix} \tag{4.1}$$

where $\mathbf{EM}$ contains $\mathbf{Z}_{11}$ $\mathbf{Z}_{12}$ $\mathbf{Z}_{21}$ and $\mathbf{Z}_{22}$ in Eqn. (3.11), $\mathbf{C'}$,$\mathbf{i'}$ and $\mathbf{v}_{\mathbf{em'}}$ are extensions of their corresponding entry in Eqn. (3.11). In Eqn. (4.1) the EM surface current and coupling current unknowns $\mathbf{i'}$ can be eliminated from the first set of equations and the rest of the system can be written in the Schur complement form:

$$\left(\mathbf{MNA} - \mathbf{C'}^{\mathbf{T}}\mathbf{EM}^{-1}\mathbf{C'}\right)\mathbf{ckt} = \mathbf{v}_{\mathbf{ckt}} - \mathbf{C'}^{\mathbf{T}}\mathbf{EM}^{-1}\mathbf{v}_{\mathbf{em'}} \tag{4.2}$$

Therefore the formal inversion of the matrix $\mathbf{EM}$ only needs to be done once as long as the EM structures do not change. For large-sized EM problems, the equivalent of the inversion is obtained by iteratively solving the EM system with each of the contacts excited independently. The EM contact representation can therefore be obtained through exciting each contact and using an iterative solver, or through the formal inversion shown in Eqn. (4.2).

The EM contact model ultimately permits the EM structure to be represented in MNA-compatible element-stamping format $\mathbf{C'}^{\mathbf{T}}\mathbf{EM}^{-1}\mathbf{C'}$ and the incident electromagnetic wave in equivalent circuit excitation format $\mathbf{C'}^{\mathbf{T}}\mathbf{EM}^{-1}\mathbf{v}_{\mathbf{em'}}$. The advantage of the above nodal contact model compared to the traditional port model is that it eliminates the intermediate step of constructing an equivalent circuit, with its associated cost, accuracy limitations, and complexity in terms of ensuring passivity.

In a converse manner, when circuits connected to EM objects remain unchanged and the EM objects are re-designed, a *CKT contact* model can be used as shown next. In effect, this is the dual of a classical port model; a "port" model for the circuit is introduced into the EM simulation. Instead of solving EM problems for a series of

excitations at each contact, the exact effects of circuit topologies and circuit sources are incorporated in this model. The CKT contact model yields

$$\left(\mathbf{EM} - \mathbf{C}'\mathbf{MNA}^{-1}\mathbf{C}'^{\mathrm{T}}\right)\mathbf{i}' = \mathbf{v}_{\mathbf{em}'} - \mathbf{C}'\mathbf{MNA}^{-1}\mathbf{v}_{\mathbf{ckt}} \tag{4.3}$$

The fully coupled scheme Eqn. (4.1), and the *EM contact* Eqn. (4.2) and *CKT contact* Eqn. (4.3) models offer the flexibility not available with regular EM port-model approaches. At the same time, the *EM contact* model defines a node-based port model similar to existing schemes. Therefore, the presented approach can be considered a super-set of existing approaches. As will be shown in the examples in Section V, this flexibility has advantages in design iteration, visualization, and mixed-physics solution.

Once the coupled EM-circuit solution is obtained via solving Eqn. (4.1, 4.2), or Eqn. (4.3), the equivalent surface current can be post-processed to extract quantities of interest. Alternatively, contributions arising within the EM interaction matrices can be separated out in order to obtain post-processed electric (capacitance), magnetic (inductance), or electromagnetic (impedance or S-parameters) characteristics. For example, for an N-conductor model wherein an $N \times N$ inductance matrix is required, each column of the inductance matrix can be derived by applying a current of one ampere to one conductor and then solve for the equivalent surface current, wherein inductance matrix entry $\mathbf{L}_{ij}$ is computed by

$$\mathbf{L}_{ij} = imag\left(\sum_{m=N_{iN1}}^{N_{iNe}} \mathbf{A}_{im} \cdot \mathbf{i}_{im}\right) \tag{4.4}$$

where $\mathbf{A}_{im}$ and $\mathbf{i}_{im}$ stands for the overall vector potential and the equivalent surface current at the m^{th} non-boundary edge of conductor i due to one ampere incident current at

conductor j. N_{iN1} and N_{iNe} represents the starting and ending indices of non-boundary edges on conductor *i*, and *imag* denotes the imaginary part.

Similarly, one column of the capacitance matrix can be derived by applying 1V on conductor j and by solving for the equivalent surface current. The capacitance matrix entry $\mathbf{C}_{ij}$ can be computed by:

$$\mathbf{C}_{ij} = imag\left(\sum_{m=N_{iN1}}^{N_{iNp}} \Phi_{im} \mathrm{Q}_{im} \right) \tag{4.5}$$

Φ_{im} and Q_{im} are the scalar potential and charge, respectively, at the m^{th} patch of i^{th} conductor , N_{iN1} and N_{iNp} represent the indices of starting and ending patches of the i^{th} conductor.

V. Applications and Results

A fully coupled EM-circuit simulator has been developed based on the above-described approach. One of the typical applications is circuit/layout co-simulation for RF electronics system design where on-chip inductors are often employed. In radio frequency circuit design, accurate characterization of the inductor is the most challenging task. Figure 5 shows the topology of a 5.6GHz differential mode Low Noise Amplifier (LNA), where several on-chip inductors are included either for the frequency selection purpose (L1 L2) or for the impedance matching purpose (L3 L4 L5 L6).

With 5.6 GHz central working frequency, performance of LNA will be affected by both the distributed effect and the cross talk of on-chip spiral inductors. The precision of two inductors L1 and L2 is most important since it affects the central frequency where the maximum gain can be derived. While the transistor sizes are fixed by the requirement

of the optimum noise figure [20] to be 123 μm, the main design task is to adjust the turns and spacing of spiral inductors to tune the resonant frequency of the LC tank to the central frequency 5.6 GHz.

Spiral inductor L1 is first simulated using the coupled solver to decide the number of turns according to the extracted equivalent inductance using Eqn. (4.4). With a total parasitic capacitance to be 105fF at node A, the inductor is designed to be 5 turns with an area of 500μm×500μm. Figure 6 shows the extracted equivalent inductance of such a single spiral inductor. Due to the radiation and inductive coupling effects, the two inductors will mutually couple, and lead to a shift in the central frequency. Figure 7 shows a series of S_{21} curves versus different distances between the two inductors: as the two inductors close in the coupling effect becomes prominent and leads to poorer performance. In actuality, the coupling effect could be used to advantage; due to the differential mode nature of the currents through the two inductors, a larger effective inductance can be realized by tight coupling between the two inductors. In other words the same inductance value could be achieved using less number of turns and thus less chip area. Some multi-level inductor designs are based on this concept.

To simulate the coupled system in frequency domain, an operating point analysis is first performed to linearize the nonlinear BSIM3 transistor model [21]. Then, a frequency sweep is performed for the range of interest. The coupled circuit-EM solver avoids the steps of port model generation, curve fitting, and equivalent passive circuit generation, which are necessary in traditional design methods. Using the presented method, not only is a higher accuracy achieved due to the exclusion of curve fitting and finite filter size

errors, but the entire process is also faster since the coupling between the EM and circuit has been automated.

The second example studies the power/ground plane voltage bounce distribution due to a high frequency noise source. Consider a typical mixed analog/digital PCB (Print Circuit Board) as shown in Figure 8. Since digital circuits are usually associated with high speed signal switching that contains lots of high frequency components, the potential difference between power and ground planes will not be equal to ideal supply voltage VDD everywhere. This is because at high frequencies, the power and ground planes need to be considered as a distributed RLC network instead of ideal conduction planes. The voltage bounce could cause digital logic circuits to malfunction. In such case de-coupling capacitors are needed to supress the peak bounce voltage.

With traditional port model based EM-circuit simulation methods, it is difficult to acquire the voltage bounce distribution information all over the plane since the potentials can only be accessed via ports. Thus deriving the spatial distribution of potential requires ports everywhere on the plane and could make the problem cumbersome or too large to solve. On the other hand, since the coupled circuit-EM solver uses equivalent surface currents as system unknowns, the voltage/field distribution can then be easily derived by a post-processing operation once the coupled system is solved.

In Figure 8, the size of the PCB board is 12cm X 8cm. At 3GHz, 1mA noise source can cause a bounce voltage distribution as shown in Figure 9. By continuously pinning down the peak bounce voltage using 10nF decoupling capacitors, peaks of the noise voltage can be isolated in local area of the noise source as shown in Figure 10 after adding approximately twenty decoupling capacitors. Note that the EM part of the

problem does not change as additional capacitors are added, and hence the factorization and storage of the EM section can be done just once if required, using the *EM port* version of the coupled system.

An alternative design approach is to design the power/ground board as shown in Figure 11, with partially split planes. Simulation results reveal that the bounce voltage localization effect was achieved even without adding decoupling capacitors, as shown in Figure 12. Further localization of bounce voltage will need a smaller number of decoupling capacitors compared to the previous example. Bounce localization shown in Figure 13 was achieved by using 9 decoupling capacitors.

The next example illustrates the ability of the proposed method to simulate on-chip decoupling capacitance and interaction with the bond wire inductance of the power network. This example is taken from [22] and is redrawn in Figure 14. The packaging and substrate are modeled by lumped circuit components, while the power ground network are retained as physical structures. In this example, the capacitance and inductance form a resonant circuit. When logic circuits switch state, the current they consume approximates an impulse function that can excite the resonant circuit. Poor choice of decoupling capacitance size will allow the resonant peak to be near the frequency of operation of the chip. This in turn will create noise that can disrupt the function of the chip.

As can be seen from the simulation result in Figure 15, the resonance frequency can be located by a frequency sweep on the coupled EM-circuit system, without any need to first obtain frequency-dependent SPICE compatible port models of the power-ground network. The advantage of the coupled circuit-EM solver is that it can reveal both the

circuit solution and EM details together. Circuit designers are provided with one level of more detailed information in the circuit design hierarchy.

V. Conclusions

In this paper a coupled circuit-EM formulation is presented. The EM solution is based on full-wave surface integral equations (EFIE), the circuit solution is based on KVL and KCL, and the coupling is ensured by charge current continuity and potential matching. The primary objective of the method is to ensure proper physics-based coupling between the circuit and the EM parts such that a coupled matrix can be formulated. While different kinds of EM and circuit port models can be derived, a fully coupled solution process will guarantee complete electrical transparency in the whole system, including all EM and circuit effects. Work in progress is aimed at extending the same approach to the time domain simulation, to include the effect of lossy conductors, and to incorporate fast multilevel solvers and fast frequency sweep methods for the coupled system.

VI. Acknowledgments

This work was partially supported by DARPA-MTO NeoCAD grant N66001-01-1-8920, NSF-CAREER grant ECS-0093102, and NSF-SRC Mixed-Signal Initiative grant CCR-0120371, and by a grant from Ansoft Corporation.

REFERENCES

[1] K. Kundert, H. Chang, D. Jefferies, G. Lamant, E. Malavasi and F. Sendig, "Design of mixed-signal systems-on-a-chip", *IEEE Trans. Computer-Aided Design of Integrated Circuits and Systems,* vol. 19, no.12, pp. 1561–1571, Dec. 2000.

[2] I. Erdin and M. Nakhla, "Mixed circuit/electromagnetic analysis of field coupling to high speed interconnects in inhomogeneous medium", *IEEE International Symposium on Electromag. Compat*., vol. 1, pp. 446-449, Aug. 1999.

[3] W. Sui, D. A. Christensen and C. H. Durney, "Extending the Two-Dimensional FDTD Method to hybrid electromagnetic systems with active and passive lumped elements", *IEEE Trans. Microwave Theory Tech.*, vol. 40, no.4, pp. 724-730, Apr. 1992.

[4] R. Khazaka and M. Nakhla, "Analysis of high-speed interconnects in the presence of electromagnetic interference", *IEEE Trans. Microwave Theory and Techniques*, vol. 46 pp. 940-947, July 1998.

[5] S. M. Rao, D. R. Wilton and A. W. Glisson, "Electromagnetic scattering by surfaces of arbitrary shape", *IEEE Trans. Antennas Propagation*, vol. AP-30, pp. 409-418, May 1982.

[6] A. Canova, M. Ottella and D. Rodger, "A coupled field-circuit approach to 3D FEM analysis of electromechanical devices", *IEEE Ninth International Conference on Electrical Machines and Drive*, pp. 71-75, Sep. 1999.

[7] M. Feliziani and F. Maradei, "Circuit-oriented FEM: Solution of circuit-field coupled problems by circuit equations", *IEEE Transactions Magnetics*, vol. 38, no. 2, Mar 2002.

[8] M. C. Costa, S. I. Nabeta and J. R. Cardoso, "Modified nodal analysis applied to electric circuits coupled with FEM in the simulation of a universal motor", *IEEE Trans. Magnetics*, vol. 36, no. 4, July 2000.

[9] S. Chun, M. Swaminathan, L. D. Smith, J. Srinivasan, Z. Jin and M. K. Iyer, "Modeling of simultaneous switching noise in high speed systems", *IEEE Transactions Advanced Packaging*, vol. 24, no. 2, May 2001.

[10] A. E. Ruehli, "Equivalent circuit models for three-dimensional multiconductor systems" *IEEE Trans. Microwave Theory and Techniques*, vol. MTT22 (3), pp. 216-221, March 1974.

[11] A. E. Ruehli, G. Antonini, J. Esch, J. Ekman, A. Mayo and A. Orlandi, "Nonorthogonal PEEC formulation for time-and frequency-domain EM and circuit modeling", *IEEE Trans. on Electromagnetic Compatibility*, Volume: 45, Issue 2, pp167-176 May 2003.

[12] A. Rong and A. C. Cangellaris, "Generalized PEEC models for three-dimensional interconnect structures and integrated passives of arbitrary shapes", *Proc. Electrical Performance of Electronic Packaging conf.*, vol. 10, pp. 225–228, Boston, MA, Oct. 2001.

[13] Y. Wang, V. Jandhyala and C. J. Shi, "Coupled Electromagnetic-Circuit Simulation of Arbitrarily-Shaped Conducting Structures", *Proc. Electrical Performance of Electronic Packaging conf.*, vol 10, pp. 233-236, Boston, Oct 2001.

[14] G. Antonini, A. Orlandi and A. E. Ruehli, "Harten's scheme for PEEC method", *IEEE International Symposium on Electromagnetic Compatibility*, pp. 340-344 vol 1, Aug. 2001.

[15] A. Odabasioglu, M. Celik and L.T. Pileggi, "PRIMA: passive reduced-order interconnect macromodeling algorithm", *Digest of IEEE/ACM Technical Papers on International Conference Computer-Aided Design*, pp58-65, Nov. 1997.

[16] D. Gope and V. Jandhyala, "An iteration-free fast multilevel solver for dense method of moment systems", *Proc. Electrical Performance of Electronic Packaging conf.*, vol 10, pp. 177-180, Boston, Oct. 2001.

[17] D. Gope, S. Chakraborty, Y. Wang, V. Jandhyala and C. J. Shi, "A Surface based 3D coupled circuit electromagnetic simulator with accurate lossy conductor modeling", *Proc. IEEE APS-URSI*, San Antonio, June 2002.

[18] S. Chakraborty and V. Jandhyala, "Evaluation of Green's Function Integrals in Conducting Media", *UWEE Technical Report no. UWEETR-2002-0016*, Aug 2002.

[19] J. Vlach, K. Singhal and Van Nostrand Reinhold, *Computer Methods for Circuit Analysis and Design*, Van Nostrand Reinhold, ISBN: 0-442-28108-0, 1983.

[20] B. Razavi, *RF Microelectronics*, Chapter 6. Prentice Hall PTR, ISBN: 0-138-87571-5 1997.

[21] Y. Cheng and C. M. Hu, *MOSFET Modeling and BSIM3 User's Guide*, Kluwer Academic Publishers, ISBN 0-7923-8575-6, Sep. 1999.

[22] N. K. Verghese, T. J. Schmerbech and D. J. Allstot, *Simulation techniques and solutions for mixed-signal coupling in intergrated circuits*, Kluwer Academic Publishers, page 160, 1995.

Figure Captions

Figure 1: Arbitrary lumped circuit connected through a contact to a 3D geometric object.

Figure 2: Concept of surface contact.

Figure 3: Connection scheme for EM and Circuit interface.

Figure 4: Definition of RWG basis function.

Figure 5: Schematic of a 5.6GHz Low Noise Amplifier.

Figure 6: Extracted inductance of a single spiral inductor.

Figure 7: S21 curve versus distance between inductors;"inf" or infinite distance corresponds to ignoring all mutual coupling between the inductors.

Figure 8: Structure of mixed signal board with noise source at the center.

Figure 9: Bounce voltage distribution at 3GHz.

Figure 10: Bounce voltage distribution at 3GHz after adding 20 decoupling capacitors.

Figure 11: Partially split power ground plane design.

Figure 12: Bounce voltage distribution at 3GHz for split power/ground Plane.

Figure 13: Bounce voltage distribution at 3GHz for split power/ground plane with 9 decoupling capacitor.

Figure 14: Chip/Package power/gnd EM-circuit co-simulation.

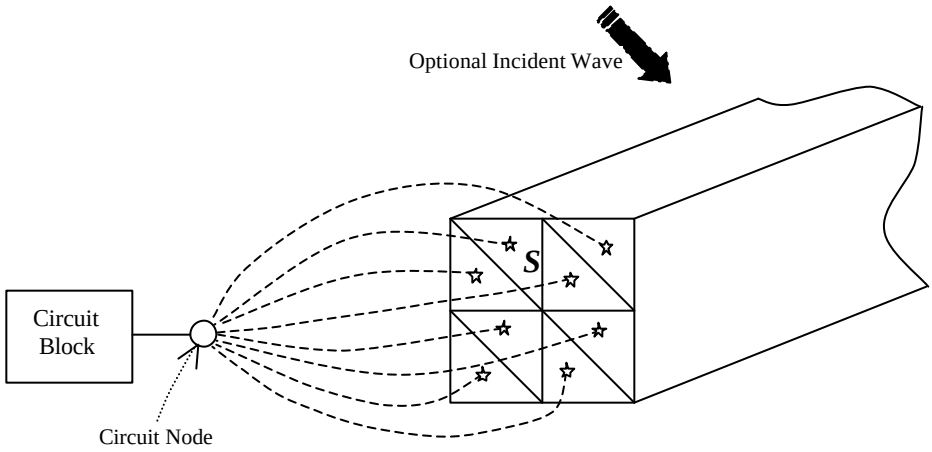

Figure 1: Arbitrary lumped circuit connected through a contact to a 3D geometric object.

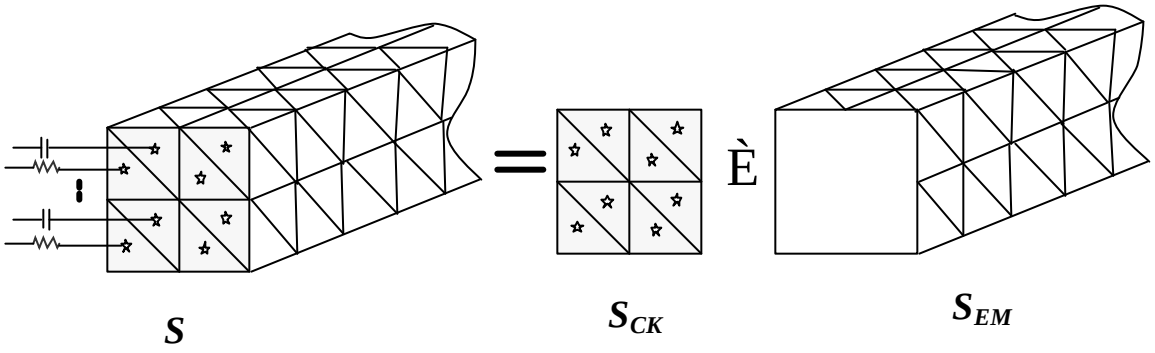

Figure 2: Concept of surface contact.

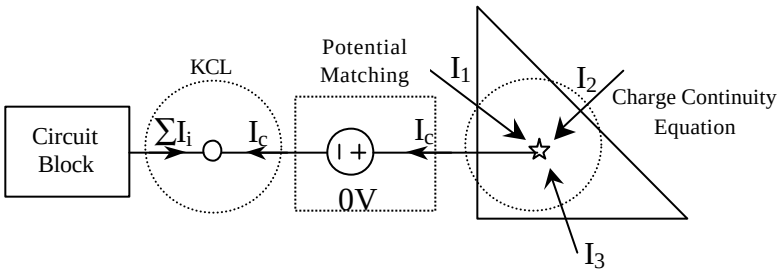

Figure 3: Connection scheme for EM and Circuit interface.

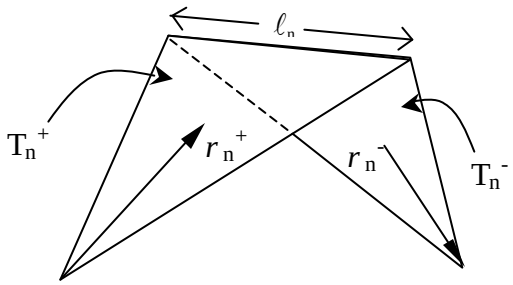

Figure 4: Definition of RWG basis function.

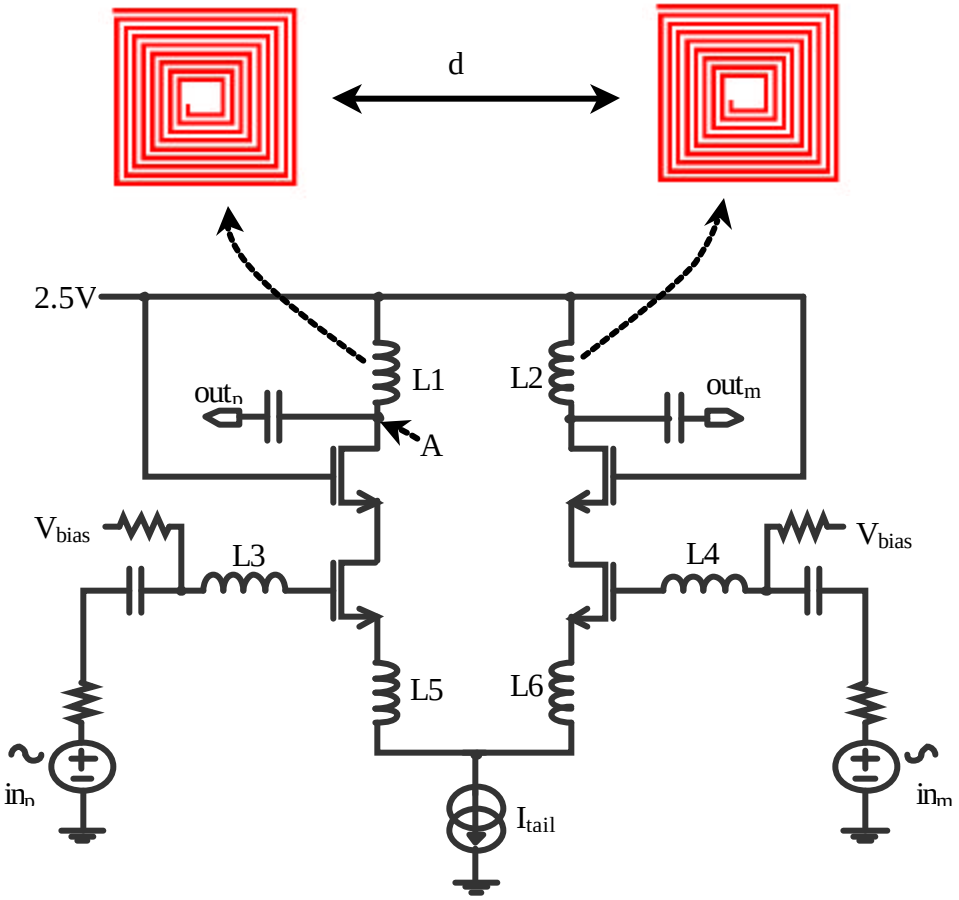

Figure 5: Schematic of a 5.6GHz Low Noise Amplifier.

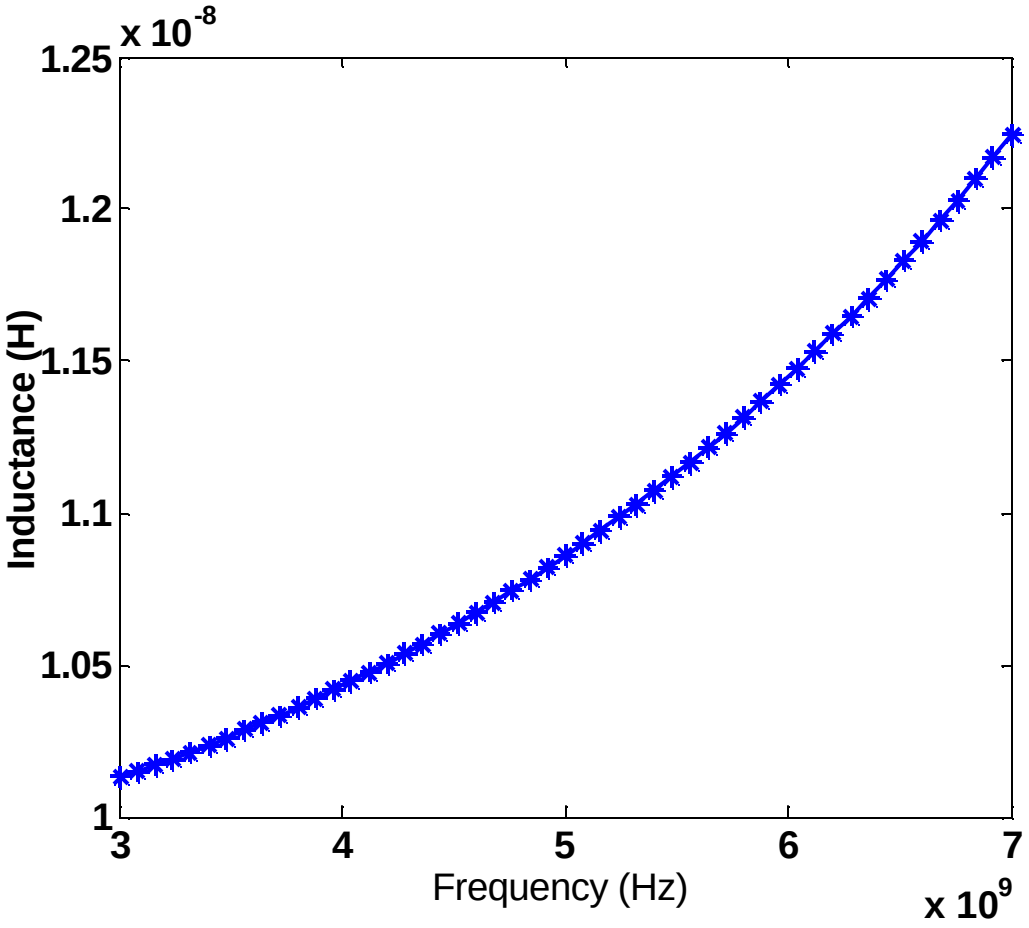

Figure 6: Extracted inductance of a single spiral inductor.

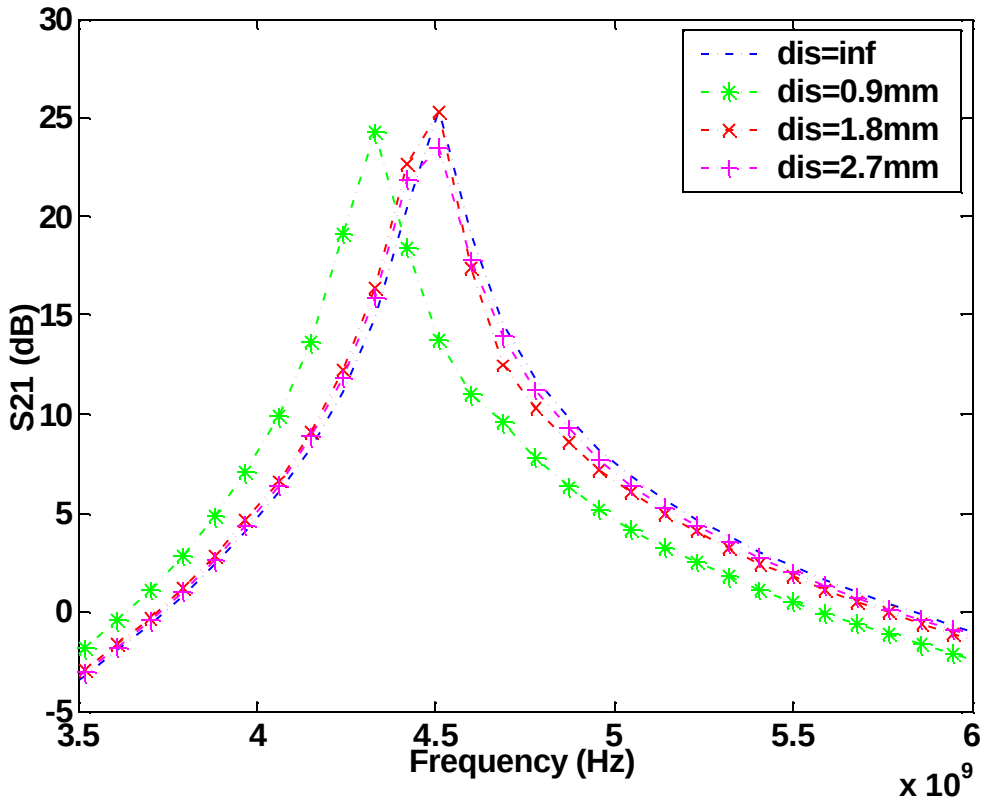

Figure 7: S21 curve versus distance between inductors ;"inf" or infinite distance corresponds to ignoring all mutual coupling between the inductors.

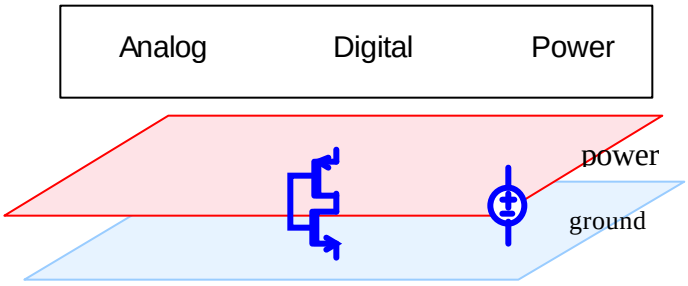

Figure 8: Structure of mixed signal board with noise source at the center.

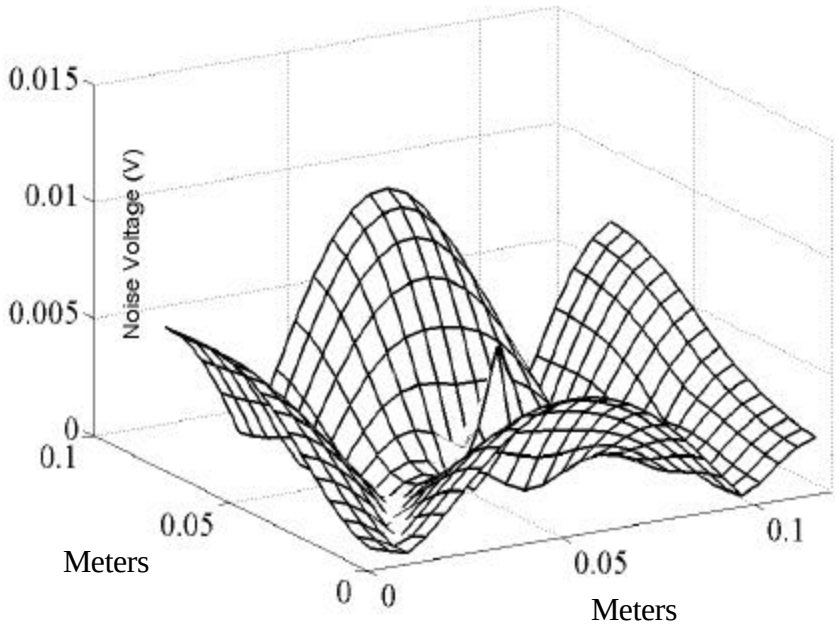

Figure 9: Bounce voltage distribution at 3GHz.

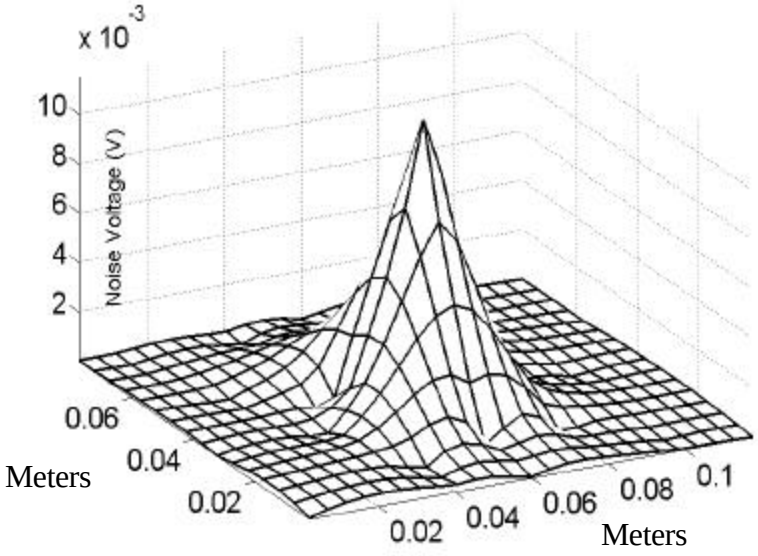

Figure 10: Bounce voltage distribution at 3GHz after adding 20 decoupling capacitors.

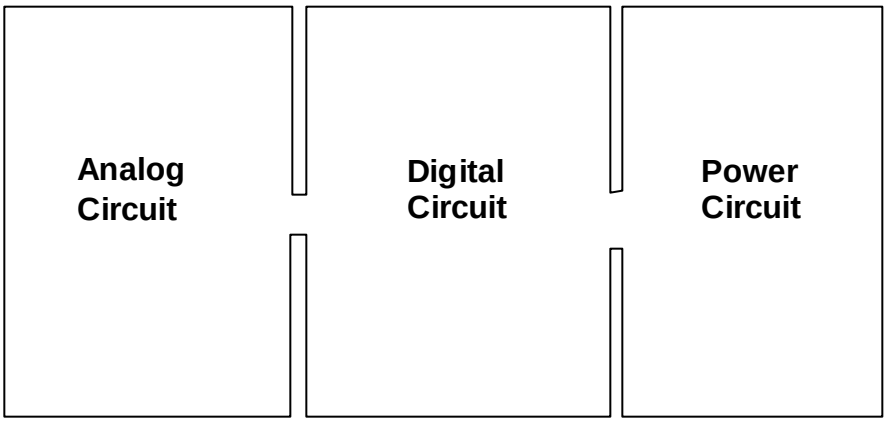

Figure 11: Partially split power ground plane design.

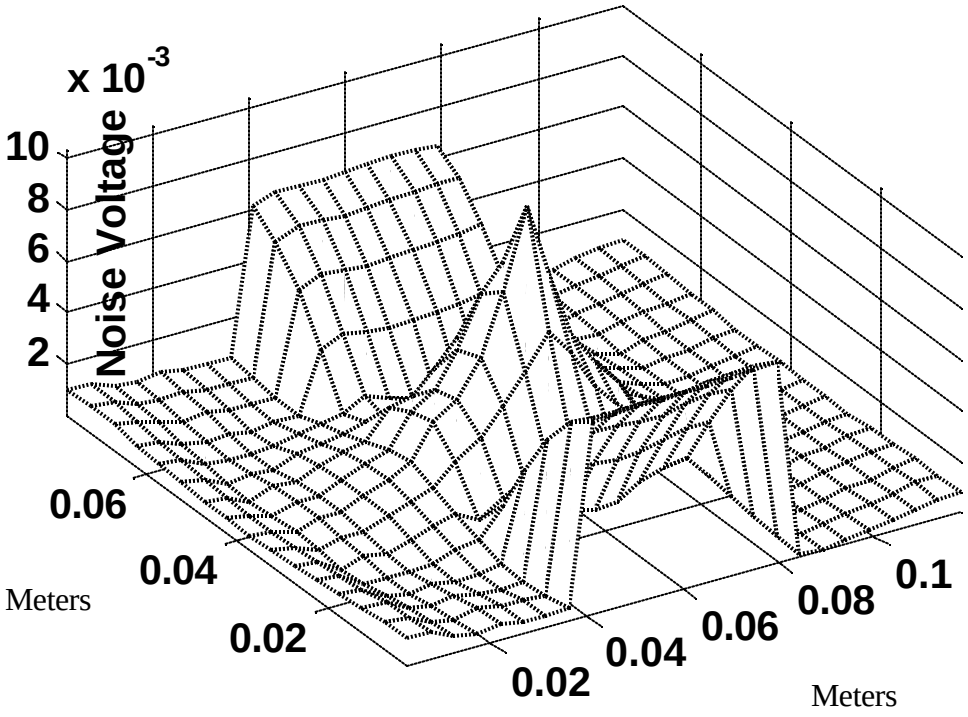

Figure 12: Bounce voltage distribution at 3GHz for split power/ground Plane.

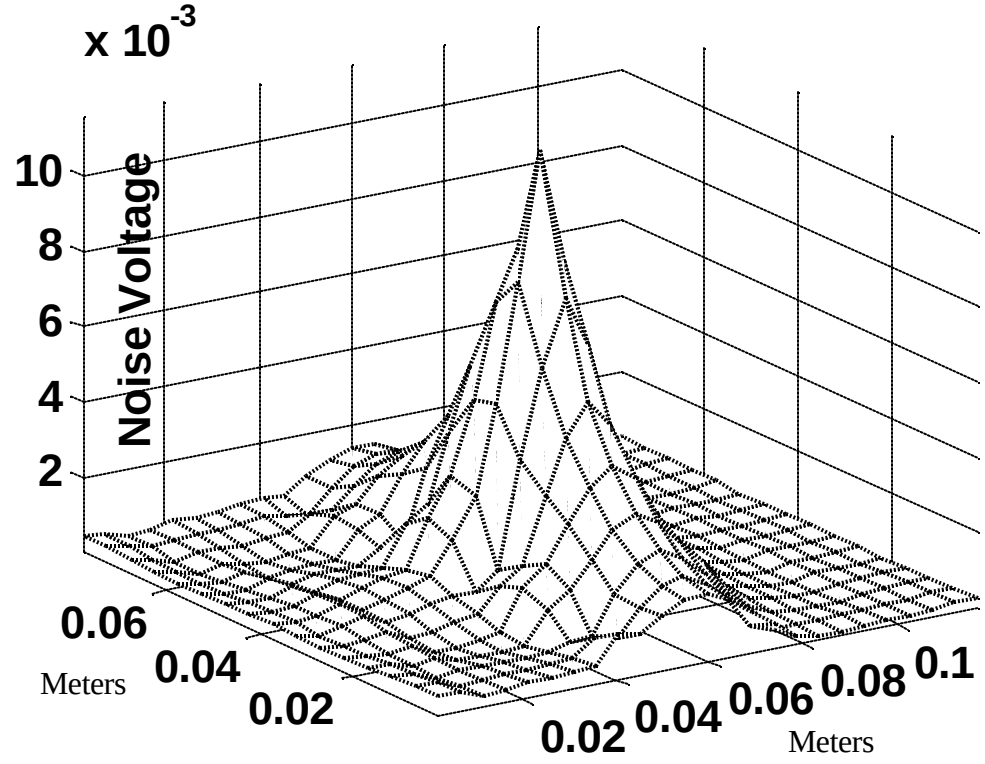

Figure 13: Bounce voltage distribution at 3GHz for split power/ground plane with 9 decoupling capacitor.

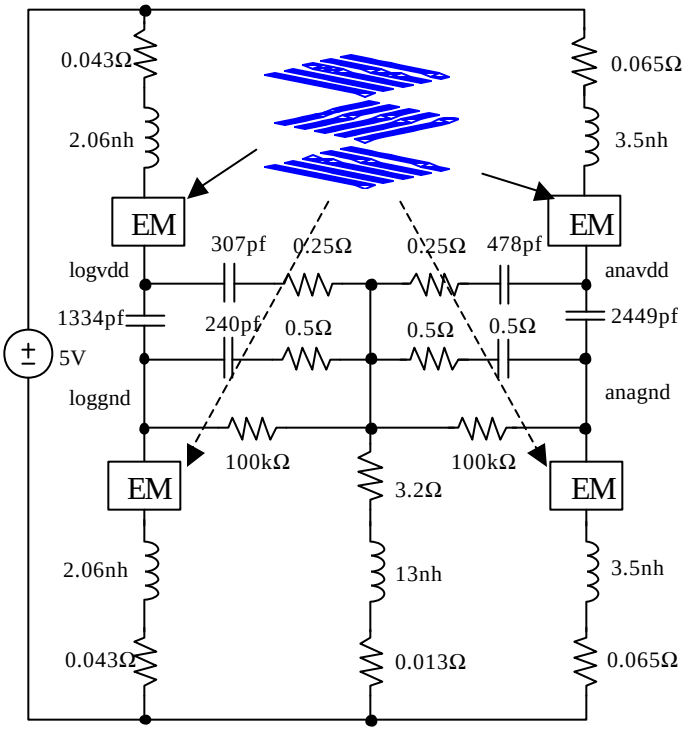

Figure 14: Chip/Package power/gnd EM-circuit co-simulation.

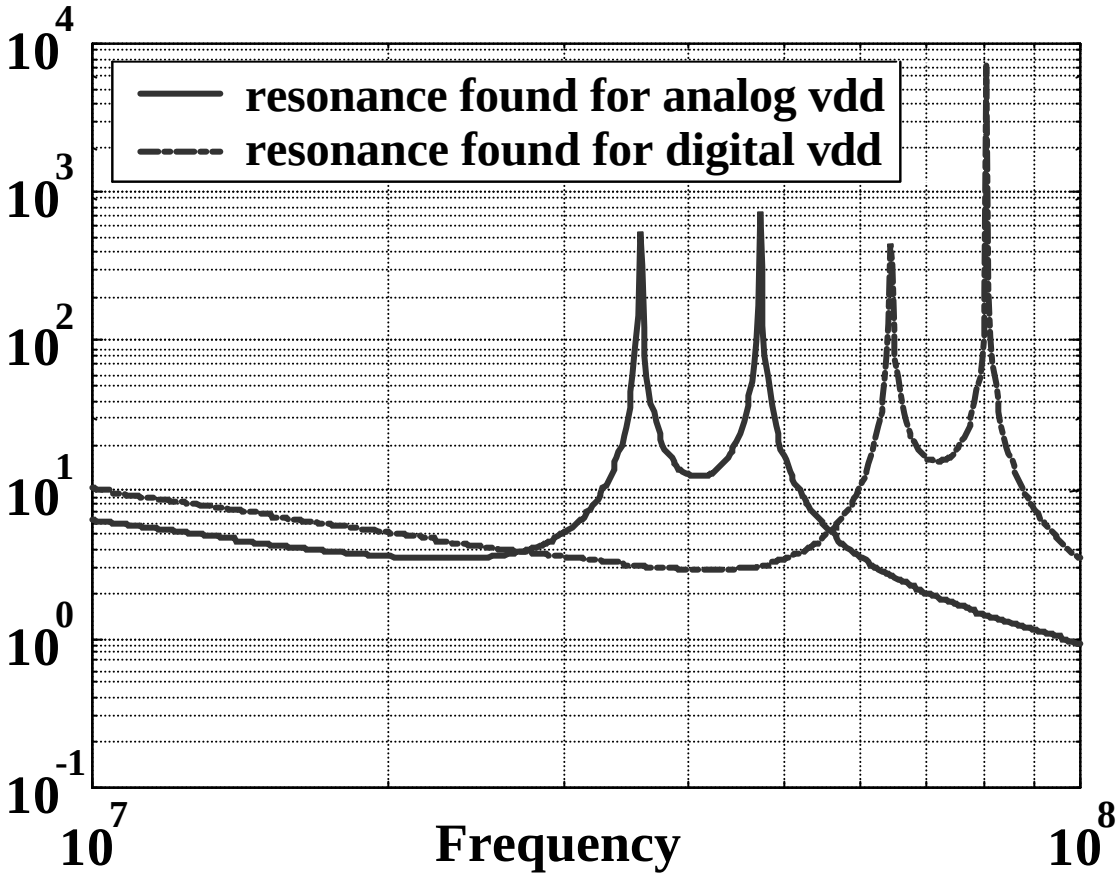

Figure 15: Resonance frequency location using coupled EM-circuit simulation.